RSC Advances

PAPER

View Article Online
View Journal | View Issue

Cite this: *RSC Adv.*, 2025, **15**, 45690

Novel thiophene–thiazole-Schiff base hybrids: design, synthesis, antimicrobial and antioxidant activity with ADMET prediction, molecular docking and dynamics study

Samira Jarin Khan,†[a] Sumita Saznin Marufa,†[a] Md. Imtiaz Sultan,[a] Alin Tasnim Aurora,[a] Joya Rani Debnath,[a] Shanta Easmin,[a] Hiroshi Nishino,[b] Md. Aminul Haque *[a] and Mohammad Mostafizur Rahman *[a]

This study was aimed to synthesize new antimicrobial and antioxidant agents with increased biological efficacy due to increasing pathogenic resistance and oxidative stress. In this context, a series of thiazole-Schiff base derivatives (**2a–k**) were synthesized *via* a two-step synthetic route (Scheme 1). The structures of the synthesized compounds were characterized using analytical methods, including IR, ^{1}H NMR, and HRMS. As part of the dual biological potential of the synthesized derivatives, *in vitro* antimicrobial studies were performed using the agar disc diffusion method, where **2f**, **2h**, and **2k** showed excellent activity against both Gram-positive and Gram-negative bacterial strains. However , compound **2f** exhibited the most prominent antimicrobial activity, especially as an antifungal-active derivative, with inhibitory values of 20.2 ± 0.6 mm (*T. harzianum*) and 32.3 ± 0.5 mm (*A. niger*), which were higher than those of standard amphotericin B (17.2 ± 0.6 mm and 8.0 ± 0.8 mm, respectively). Furthermore, the antioxidant activity of the synthesized compounds was evaluated by DPPH free radical assays, where compounds **2b** and **2c** exhibited potent antioxidant activity, with IC_{50} values of 31.10 ± 3.57 μg mL^{-1} and 14.78 ± 2.73 μg mL^{-1}, respectively, compared with that of standard ascorbic acid (49.67 ± 4.63 μg mL^{-1}). Complementary *in silico* physicochemical and pharmacokinetic properties with drug-likeness and toxicological parameters were computed and analyzed. Moreover, molecular docking studies and MD simulations were performed for the selected complexes to explore their possible binding interactions and stability.

Received 27th September 2025
Accepted 10th November 2025

DOI: 10.1039/d5ra07357j

rsc.li/rsc-advances

1. Introduction

Infectious diseases continue to pose a severe global threat to the public health due to their ability to spread quickly across populations and their high mortality rates, particularly in low- and middle-income countries.[1] The widespread use of antimicrobial agents has historically mitigated the impact of microbial infections. However, the rise of antimicrobial resistance (AMR) has significantly decreased the efficacy of many existing therapies, prompting an urgent need for new drug development strategies.[2,3] Traditional measures like improving hygiene or modifying lifestyles are insufficient to combat AMR. A more effective approach involves the discovery of novel antimicrobial agents with unique mechanisms of action.[4,5] One promising strategy is the design of hybrid molecules that incorporate multiple bioactive pharmacophores to enhance biological activity and circumvent resistance pathways. Among heterocyclic compounds, thiazole, which contains nitrogen and sulfur atoms in a five-membered ring, has demonstrated a broad spectrum of pharmacological properties, including antimicrobial, antiviral, anti-inflammatory, anticancer, antioxidant, and antihypertensive activities.[6–13] Moreover, the core structure of penicillin, the first widely used antibiotic, has a tetrahydrothiazole group and a lactam ring, emphasizing its relevance in pharmacology. Thiophene, another sulfur-containing, five-membered heterocycle, is known for its high electron density and polarizability, which enhance its binding affinity to various biological targets. It is also capable of influencing the half-life of drugs, ADME properties, and permeability owing to the presence of the sulfur atom in its structure. Thiophene derivatives possess diverse biological activities, encompassing anti-inflammatory, antimicrobial, anticancer, anti-HIV, antidepressant, and antitubercular activities,[14–20] which place thiophene as a prime synthetic scaffold for future drug regimens.

[a]*Department of Chemistry, Jagannath University, Dhaka 1100, Bangladesh. E-mail: amin2k12@chem.jnu.ac.bd; mostafiz@chem.jnu.ac.bd*

[b]*Department of Chemistry, Graduate School of Science and Technology, Kumamoto University, Kumamoto, Japan*

† Samira Jarin Khan and Sumita Saznin Marufa have equal contribution as first authors.

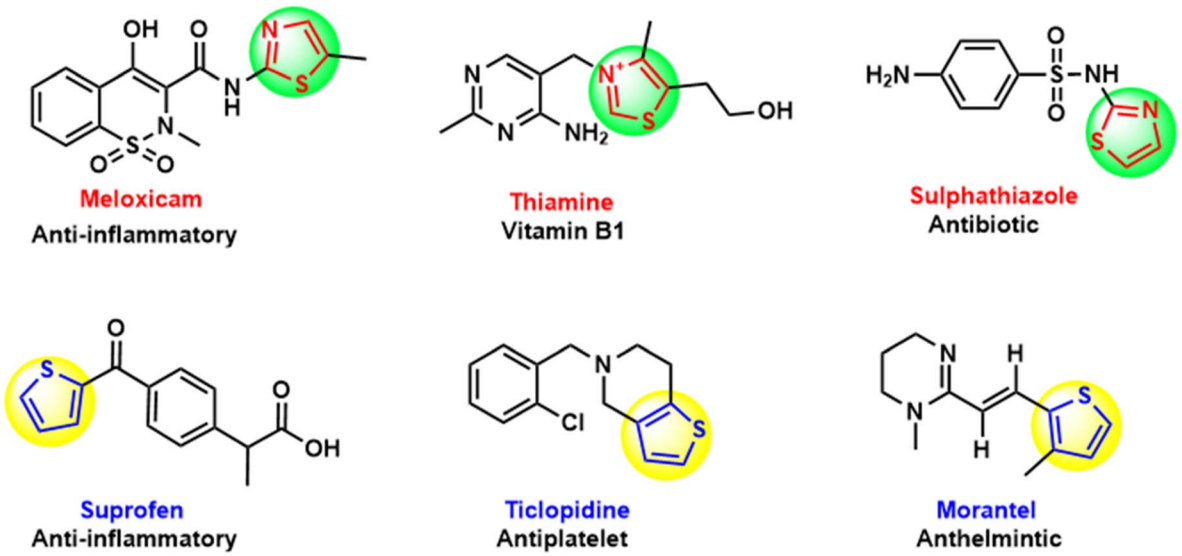

Fig. 1 Examples of some reported thiazole- and thiophene-containing derivatives. Red and blue representations indicate thiazole and thiophene moieties, respectively.

Some commercial drugs, such as cefotaxime (antimicrobial agent), penthiopyrad (fungicide), raltitrexed (anticancer), thiophenfurin (anti-tumor), and tiamenidine (antihypertension), possess therapeutic potential for future drug design (Fig. 1). Similarly, Schiff bases, first reported by Hugo Schiff in 1864, have gained prominent interest due to their structural flexibility and pharmacological relevance. Schiff-base derivatives have demonstrated significant bioactivities in various therapeutic fields, including antimicrobial, anticancer, and antiviral applications.[21–24] Notable examples of commercially available drugs include thioacetazone (antitubercular), triapine (anticancer), and methisazone (antiviral). By considering the structural and therapeutic importance of thiazole, thiophene, and Schiff-base scaffolds, the current study focuses on the design and synthesis of novel hybrid compounds integrating these three pharmacophores, which would be a feasible step in the discovery of new synthetic approaches and addressing the current crisis of AMR. In addition, the antioxidant capability of the novel derivatives was evaluated to address oxidative stress and various chronic diseases, such as cancer and skin disorders.[12] The disc diffusion method was applied for the antimicrobial screening of the novel analogs, and an antioxidant experiment was conducted using the DPPH free radical scavenging assay. As part of the investigation and the advancement of drug design, *in silico* studies were performed, which included ADMET prediction, optimization, molecular docking, and molecular dynamics simulations for predicting the oral bioavailability, binding interactions within receptor proteins, and the stability of protein–ligand complexes.

2. Materials and methods

2.1 General method

All the reactants and initiating chemicals were obtained from commercially available sources and were used without additional purification. The melting points of the synthesized compounds were measured in open capillary tubes using a Stuart-SMP10 melting point instrument and were uncorrected. The progress of the reactions was monitored by thin-layer chromatography (TLC) using aluminum sheets coated with silica gel $60F_{254}$ (Merck, Germany), and detection was achieved by exposure to UV light. Recrystallization was performed for the purification of the products. The IR spectra were acquired on a SHIMADZU IR Tracer-100 infrared spectrophotometer using KBr pellets, and the values were expressed in cm^{-1}. The ^1H NMR spectra were acquired on a BRUKER NMR spectrometer at 400 MHz in DMSO-d_6 as a solvent containing TMS as an internal standard, and the values were expressed in parts per million (ppm). The mass spectra were acquired using a JEOL JMS-700 MStation from the Instrumental Analysis Centre, Kumamoto University, Kumamoto, Japan.

2.2 Synthesis

2.2.1 Synthesis of 5-methylthiophene-2-carboxaldehydethiosemicarbazone (1a). The reaction was started by an equimolar mixture of thiosemicarbazide (0.001 mol) and 5-methylthiophene-2-carboxaldehyde (0.001 mol), with stirring in ethanol (10 mL) under reflux conditions at 80 °C until the reaction was completed. The reaction was continued until completion (checked through TLC). After the reaction, the mixture was cooled to room temperature. The crude product was filtered and recrystallized with ethanol to yield 5-methylthiophene-2-thiosemicarbazone.[25]

2.2.2 General procedure for synthesis of 2-{2-[(5-methylthiophen-2-yl)methylidene]hydrazin-1-yl}-1,3-thiazoles 2a–k. A mixture of 5-methylthiophene-2-thiosemicarbazone (**1a**) (0.0997 g, 0.5 mmol) was dissolved in 10 mL of acetone with α-haloketone derivatives (0.5 mmol). The mixture was refluxed with stirring at 60 °C for 3–25 hours. The progress of the

reaction was checked using TLC. After completion, the mixture was left at room temperature, and the crude residue was collected by filtration. The crude residue was then recrystallized from ethanol to yield the pure final products **2a–k** (Scheme 1).

*2.2.2.1 Ethyl-2-{2-[2-[(5-methylthiophen-2-yl)methylidene] hydrazin-1-yl}-1,3-thiazol-4-yl)acetate (**2a**).* Black solid, yield (64%); R_f value = 0.676 (EtOAc : hexane = 3 : 4); m. p. = 130–132 °C. IR (KBr, ν_{max}, cm^{-1}): 3407 (NH), 1717 (C=O), 1624 (C=N), 1220 (C–O–C), 731 (C–S–C). ^1H NMR (400 MHz, δ, ppm, DMSO-d_6): 1.20 (d, 3H, J = 6.4 Hz, CH_3), 2.45 (s, 3H, CH_3), 3.64 (s, 2H, CH_2), 4.09 (d, 2H, J = 6.8 Hz, CH_2), 6.71 (s, 1H, Ar–H), 6.81 (s, 1H, Ar–H), 7.21 (s, 1H, Ar–H), 8.24 (s, 1H, N=CH). FAB HRMS (acetone/NBA) calcd for $C_{13}H_{16}N_3O_2S_2$ 310.0684 $[M + H]^+$. Found: 310.0680.

*2.2.2.2 1-(4-Methyl-2-{2-[(5-methylthiophen-2-yl)methylidene] hydrazin-1-yl}-1,3-thiazol-5-yl)ethan-1-one (**2b**).* Brown solid, yield (85%); R_f value = 0.763 (EtOAc : hexane = 3 : 4); m. p. = 202–203 °C. IR (KBr, ν_{max}, cm^{-1}): 3404 (NH), 1680 (C=O), 1627 (C=N), 735 (C–S–C). ^1H NMR (400 MHz, δ, ppm, DMSO-d_6): 2.39 (s, 3H, CH_3), 2.45 (s, 3H, CH_3), 2.47 (s, 3H, $COCH_3$), 6.81 (d, 1H, J = 2.8 Hz, Ar–H), 7.21 (d, 1H, J = 3.2 Hz, Ar–H), 8.21 (s, 1H, N=CH). FAB HRMS (acetone/NBA) calcd for $C_{12}H_{14}N_3OS_2$ 280.0578 $[M + H]^+$. Found: 280.0576.

*2.2.2.3 Ethyl-2-{2-[(5-methylthiophen-2-yl)methylidene] hydrazin-1-yl}-4-methyl-1,3-thiazole-5-carboxylate (**2c**).* Brown solid, yield (76%); R_f value = 0.553 (EtOAc : hexane = 3 : 4); m. p. = 193–194 °C. IR (KBr, ν_{max}, cm^{-1}): 3453 (NH), 1717 (C=O), 1638 (C=N), 733 (C–S–C). ^1H NMR (400 MHz, δ, ppm, DMSO-

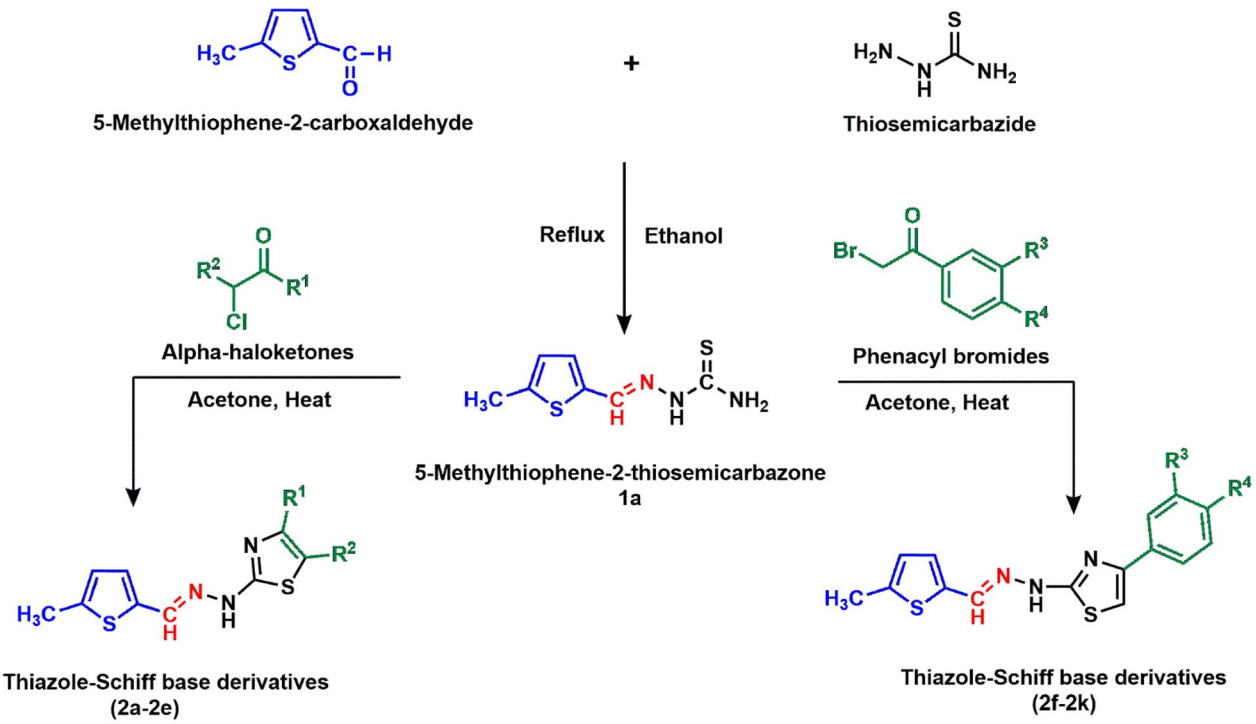

Compound	R^1	R^2
2a	$CH_2COOC_2H_5$	H
2b	CH_3	$COCH_3$
2c	CH_3	$COOC_2H_5$
2d	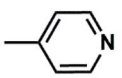	H
2e	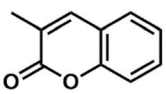	H

Compound	R^3	R^4
2f	H	H
2g	H	CH_3
2h	H	OCH_3
2i	NO_2	H
2j	H	NO_2
2k	Cl	Cl

Scheme 1 Synthesis of thiophene-containing thiazole-Schiff base derivatives.

d_6): 1.26 (t, 3H, J = 7.2 Hz, CH_3), 2.45 (s, 3H, CH_3), 2.49 (s, 3H, CH_3), 4.18 (q, 2H, J = 7.2 Hz, CH_2), 6.81 (s, 1H, Ar–H), 7.21 (s, 1H, Ar–H), 8.19 (s, 1H, N=CH). FAB HRMS (acetone/NBA) calcd for $C_{13}H_{16}N_3O_2S_2$ 310.0684 $[M + H]^+$. Found: 310.0681.

*2.2.2.4 3-{2-{2-[(5-Methylthiophen-2-yl)methylidene]hydrazin-1-yl}-1,3-thiazol-4-yl)pyridine (**2d**).* Brown solid, yield (81%); R_f value = 0.541 (EtOAc : hexane = 5 : 2); m. p. = 200–201 °C. IR (KBr, ν_{max}, cm^{-1}): 3384 (NH), 1638 (C=N), 732 (C–S–C). ^1H NMR (400 MHz, δ, ppm, DMSO-d_6): 2.46 (s, 3H, CH_3), 6.81 (m, 1H, Ar–H), 7.19 (d, 1H, J = 3.6 Hz, Ar–H), 7.81 (s, 1H, Ar–H), 8.04 (m, 1H, Ar–H), 8.18 (s, 1H, N=CH), 8.85–8.78 (m, 2H, Ar–H), 9.21 (d, 1H, J = 2 Hz, Ar–H). FAB HRMS (acetone/NBA) calcd for $C_{14}H_{13}N_4S_2$ 301.0582 $[M + H]^+$. Found: 301.0587.

*2.2.2.5 3-(2-{2-[(5-Methylthiophen-2-yl)methylidene]hydrazin-1-yl}-1,3-thiazol-4-yl)-2H-chromen-2-one (**2e**).* Yellow solid, yield (90%); R_f value = 0.410 (EtOAc : hexane = 3 : 4); m. p. = 247–248 °C. IR (KBr, ν_{max}, cm^{-1}): 3158 (NH), 1719 (C=O), 1627 (C=N), 756 (C–S–C). ^1H NMR (400 MHz, δ, ppm, DMSO-d_6): 2.46 (s, 3H, CH_3), 6.79 (s, 1H, Ar–H), 7.17 (s, 1H, Ar–H), 7.37–7.46 (m, 2H, Ar–H), 7.63 (t, 1H, J = 7.6 Hz, Ar–H), 7.75 (s, 1H, Ar–H), 7.85 (d, 1H, J = 7.6 Hz, Ar–H), 8.16 (s, 1H, Ar–H), 8.53 (s, 1H, N=CH). FAB HRMS (acetone/NBA) calcd for $C_{18}H_{14}N_3O_2S_2$ 368.0527 $[M + H]^+$. Found: 368.0529.

*2.2.2.6 2-{2-[(5-Methylthiophen-2-yl)methylidene]hydrazin-1-yl}-4-phenyl-1,3-thiazole (**2f**).* Brown solid, yield (92%); R_f value = 0.436 (EtOAc : hexane = 2 : 5); m. p. = 216–217 °C. IR (KBr, ν_{max}, cm^{-1}): 3419 (NH), 1624 (C=N), 747 (C–S–C). ^1H NMR (400 MHz, δ, ppm, DMSO-d_6): 2.26 (s, 3H, CH_3), 6.78–6.79 (m, 1H, Ar–H), 7.15 (d, 1H, J = 3.6 Hz, Ar–H), 7.28–7.32 (m, 2H, Ar–H), 7.38–7.42 (m, 2H, Ar–H), 7.82–7.84 (m, 2H, Ar–H), 8.13 (s, 1H, N=CH). FAB HRMS (acetone/NBA) calcd for $C_{15}H_{14}N_3S_2$ 300.0629 $[M + H]^+$. Found: 300.0617.

*2.2.2.7 2-{2-[(5-Methylthiophen-2-yl)methylidene]hydrazin-1-yl}-4-(4-methylphenyl)-1,3-thiazole (**2g**).* Cream-colored solid, yield (88%); R_f value = 0.718 (EtOAc : hexane = 3 : 4); m. p. = 237–238 °C. IR (KBr, ν_{max}, cm^{-1}): 3038 (NH), 1620 (C=N), 756 (C–S–C). ^1H NMR (400 MHz, δ, ppm, DMSO-d_6): 2.31 (s, 3H, CH_3), 2.61 (s, 3H, CH_3), 6.78–6.79 (m, 1H, Ar–H), 7.15 (d, 1H, J = 3.6 Hz, Ar–H), 7.19–7.26 (m, 3H, Ar–H), 7.71 (d, 2H, J = 8.4 Hz, Ar–H), 8.14 (s, 1H, N=CH). FAB HRMS (acetone/NBA) calcd for $C_{16}H_{16}N_3S_2$ 314.0786 $[M + H]^+$. Found: 314.0786.

*2.2.2.8 2-{2-[(5-Methylthiophen-2-yl)methylidene]hydrazin-1-yl}-4-(4-methoxyphenyl)-1,3-thiazole (**2h**).* Brown solid, yield (81%); R_f value = 0.615 (EtOAc : hexane = 1 : 2); m. p. = 197–198 °C. IR (KBr, ν_{max}, cm^{-1}): 3409 (NH), 1622 (C=N), 736 (C–S–C). ^1H NMR (400 MHz, δ, ppm, DMSO-d_6): 2.45 (s, 3H, CH_3), 3.77 (s, 3H, OCH_3), 6.78–6.79 (m, 1H, Ar–H), 6.94–6.97 (m, 2H, Ar–H), 7.10 (s, 1H, Ar–H), 7.14 (d, 2H, J = 3.2 Hz, Ar–H, thiazole-H), 7.73–7.77 (m, 2H, Ar–H), 8.13 (s, 1H, N=CH). FAB HRMS (acetone/NBA) calcd for $C_{16}H_{16}N_3OS_2$ 330.0735 $[M + H]^+$. Found: 330.0749.

*2.2.2.9 2-{2-[(5-Methylthiophen-2-yl)methylidene]hydrazin-1-yl}-4-(3-nitrophenyl)-1,3-thiazole (**2i**).* Orange solid, yield (68%); R_f value = 0.538 (EtOAc : hexane = 1 : 3); m. p. = 242–243 °C. IR (KBr, ν_{max}, cm^{-1}): 3427 (NH), 1623 (C=N), 1353 (N=O), 739 (C–S–C). ^1H NMR (400 MHz, δ, ppm, DMSO-d_6): 2.46 (s, 3H, $-CH_3$), 6.80 (s, 1H, Ar–H), 7.16 (d, J = 2.8 Hz, 1H, Ar–H), 7.61 (s, 1H, Ar–H), 7.70 (t, J = 8 Hz, 1H, Ar–H), 8.13 (s, 1H, Ar–H), 8.15 (s, 1H, Ar–H), 8.28 (d, J = 8.0 Hz, 1H, Ar–H), 8.65 (s, 1H, –N=CH–). FAB HRMS (acetone/NBA) calcd for $C_{15}H_{13}N_4O_2S_2$ 345.0480 $[M + H]^+$. Found: 345.0471.

*2.2.2.10 2-{2-[(5-Methylthiophen-2-yl)methylidene]hydrazin-1-yl}-4-(4-nitrophenyl)-1,3-thiazole (**2j**).* Orange solid, yield (92%); R_f value = 0.231 (EtOAc : hexane = 3 : 4); m. p. = 234–345 °C. IR (KBr, ν_{max}, cm^{-1}): 3406 (NH), 1627 (C=N), 1341 (N=O), 739 (C–S–C). ^1H NMR (400 MHz, δ, ppm, DMSO-d_6): 2.45 (s, 3H, CH_3), 6.78–6.80 (m, 1H, Ar–H), 7.16 (d, 1H, J = 1.6 Hz, Ar–H), 7.67 (s, 1H, Ar–H), 8.07–8.10 (m, 2H, Ar–H), 8.14 (s, 1H, N=CH), 8.24–8.28 (m, 2H, Ar–H). FAB HRMS (acetone/NBA) calcd for $C_{15}H_{13}N_4O_2S_2$ 345.0480 $[M + H]^+$. Found: 345.0473.

*2.2.2.11 2-{2-[(5-Methylthiophen-2-yl)methylidene]hydrazin-1-yl}-4-(3,4-dichlorophenyl)-1,3-thiazole (**2k**).* Light yellow color solid, yield (76%); R_f value = 0.462 (EtOAc : hexane = 1 : 4); m. p. = 245–246 °C. IR (KBr, ν_{max}, cm^{-1}): 3409 (NH), 1622 (C=N), 734 (C–S–C). ^1H NMR (400 MHz, δ, ppm, DMSO-d_6): 2.45 (s, 3H, CH_3), 6.79 (d, 1H, J = 3.6 Hz, Ar–H), 7.16 (d, 1H, J = 3.6 Hz, Ar–H), 7.51 (s, 1H, Ar–H), 7.65 (d, 1H, J = 8.4 Hz, Ar–H), 7.82 (m, 1H, Ar–H), 8.06 (d, 1H, J = 2.0 Hz, Ar–H), 8.13 (s, 1H, N=CH). FAB HRMS (acetone/NBA) calcd for $C_{15}H_{12}Cl_2N_3S_2$ 367.9850 $[M + H]^+$. Found: 367.9835.

2.3 Antimicrobial activity assay

The *in vitro* antimicrobial activity was assessed using the agar disc diffusion method.[26] Mueller–Hinton agar (for bacteria) and potato dextrose agar (for fungi) were used as the media for culturing the tested organisms. The aptitude of the synthesized compounds was assessed against four Gram-positive bacteria, *S. aureus* (cars-2), *B. megaterium* (ATCC-9855), *B. cereus* (carsgp-1), and *B. subtilis* (carsgp-3), two-Gram negative bacteria, *E. coli* (carsgn-2) and *S. typhi* (K-323130), and two fungal strains, *A. niger* (carsm-3) and *T. harzianum* (carsm-2). After 24 hours of incubation of the agar plates, the tested organisms were inoculated into the broth media using a sterilized cotton bar. Before injecting the sample solution, the sterilized discs were placed on the cultured media plates. Three milligrams of the sample were dissolved in 500 μL of the DMSO solution. In each disc, 50 μL of the dissolved sample was injected using a micropipette. Ceftriaxone (for bacteria) and amphotericin B (for fungi) were used (10 μL) as standards for comparing the activities of the synthesized analogs. After injecting the tested compounds, 24 hours of incubation was performed at 37 °C for assessing the antibacterial activity and 48 hours at 26 °C for assessing the antifungal activity before the inhibitory zone measurements.

2.4 Antioxidant activity

The antioxidant potential of the synthesized compounds was determined using the DPPH (2,2-diphenyl-1-picrylhydrazyl) radical scavenging method.[27] In this method, 3 mg of the DPPH powder was stirred in methanol (500 mL) in a volumetric flask (covered with aluminum foil) for 2 hours to prepare the free radical stock solution. For a single compound, 4 mL of the stock solution was transferred into five different test tubes with the following concentrations: 15, 30, 60, 150, and 250 μg mL^{-1}.

The prepared sample solution (100 μL) in methanol was added to each test tube. The mixture of the free radicals and the sample solution was kept for 20 minutes in a dark environment for a better reaction. After the dark condition, the mixture was vortexed and analyzed with a UV-spectrophotometer (SHIMADZU) to measure the percentage of inhibition of the new molecules and the standard (ascorbic acid) using absorbance at a 517 nm. This procedure was repeated three times for both the synthesized compounds and the standard. The percentage of inhibition was calculated using eqn (1):

$$\text{Inhibition}(\%) = \frac{A_{\text{control}} - A_{\text{sample}}}{A_{\text{control}}} \times 100 \quad (1)$$

where A_{control} = absorbance of DPPH radicals and A_{sample} = absorbance of DPPH with samples. The IC_{50} values for ascorbic acid and synthesized compounds were deduced from the concentration-inhibition curves.

2.5 Computational studies

2.5.1 Molecular docking study. To comprehend the binding affinity and structural details of the newly synthesized compounds, molecular docking was performed against different protein receptors. The synthesized analogs were optimized by the DFT method on the basis set of B3LYP/6-31+G(d,p) using Gaussian 16W software. Before docking, the energy was minimized, and the non-essential residues were removed from the selected protein structure using Swiss-PdbViewer and the PyMOL software, respectively. Finally, the clean, optimized structures were processed in the PyRx software for molecular docking *via* AutoDock Vina. Four different protein co-crystals were considered in this study, namely, *B. subtilis* (PDB ID: **8ARE**),[28] *S. typhi* (PDB ID: **3G1T**),[29] *A. niger* (PDB ID: **5LWX**),[30] and the human antioxidant enzyme receptor (PDB ID: **2CDU**)[31] based on *in vitro* experiments. The requisite proteins were acquired from the RCSB Protein Data Bank (**https://www.rcsb.org**). BIOVIA Discovery Studio provided the visualized structure and captured the 3D and 2D images of the docked complexes.

2.5.2 *In silico* ADMET properties. Regarding the oral bioavailability and the detrimental effects of the synthesized derivatives, three online web tools (Admetlab 2.0, Swiss ADME, and Osiris Property Explorer) were used.[32,33] Swiss ADME and Admetlab 2.0 were used for calculating the ADME (absorption, distribution, metabolism, and excretion) properties of the new derivatives along with the standards. Additionally, the overall toxicities, drug-likeness, and the drug scores of the synthesized compounds with standards were estimated using Osiris Property Explorer. The absorption percentage (%ABS) was derived from the following equation:

$$\%\text{ABS} = 109 - (0.3459 \times \text{TPSA}) \quad (2)$$

where TPSA is the topological polar surface area.

2.5.3 Molecular dynamics (MD) simulation. MD simulations offer a novel comprehension of the dynamic behaviors of molecules and interactions at the atomic scale. This method furnishes robust frameworks for understanding how stable a ligand is inside a protein binding pocket and its conformational changes. It is a vital step for facilitating logical drug design processes. Four ligand–protein complexes were simulated for 25 ns using the YASARA software, version 22.9.24.W.64 bar. Energy minimization was conducted through an optimized step for acquiring an equilibrated system. During the simulation, pH 7.4 was sustained, along with the addition of NaCl (0.9%) for neutralization. The complex was introduced inside a periodic boundary with 1.0 bar pressure at a temperature of 300 K and a water density of 0.997 g mL^{-1} was preserved. AMBER14 forcefield with 250 snapshots, each for 100 picoseconds, was used for analyzing and calculating the corresponding trajectory.[34]

3. Results and discussion

3.1 Chemistry

In this study, eleven novel thiophene–thiazole-Schiff base derivatives (**2a–k**) were synthesized *via* a two-step reaction. In the first step, 5-methylthiophene-2-carboxaldehyde and thiosemicarbazide were refluxed with stirring at 78 °C in an ethanol solution. The initial product (**1a**) from the first step interacted with the alpha-haloketones or phenacyl bromides, forming the desired final compounds. Different characterization techniques (IR, ^{1}H NMR, and HRMS) were used for confirming the structures of the synthesized analogs. The spectroscopic characterization of compound **2c** was described; for instance, its IR absorption peaks were found at 3453, 1717, 1638, and 733 cm^{-1}, confirming the presence of NH, C=O, C=N, and C–S–C functional groups.[35,36] In the ^{1}H NMR spectrum, a singlet was observed at 8.19 ppm for the azomethene group. Additionally, the aromatic ring containing two protons appeared at 6.81 ppm and 7.21 ppm with two individual singlets. Only the quartet in the spectrum was visible at 4.18 ppm due to the presence of CH_2 in the thiazole ring substituent of the ether group. The methyl group in the substituted ether showed a triplet at 1.26 ppm with a coupling constant of 7.2 Hz. Moreover, the methyl groups in the thiophene and thiazole rings displayed two singlets at 2.45 ppm and 2.49 ppm, respectively. The calculated HRMS data confirmed the exact mass of the desired derivatives.

3.2 Antimicrobial activity

The *in vitro* antimicrobial activities of the novel thiazole-Schiff base derivatives were evaluated against four Gram-positive bacteria (*S. aureus*, *B. megaterium*, *B. cereus*, and *B. subtilis*), two Gram-negative bacteria (*E. coli* and *S. typhi*), and two fungi (*T. harzianum* and *A. niger*) using the agar disc diffusion method. The zone of inhibition values of the derivatives and standards are depicted in Table 1. Most of the new chemical entities revealed potential bioactivities with moderate-to-high inhibitory values against all the bacterial and fungal strains. The presence of the thiazole-Schiff base derivatives improved the mechanism of protein binding owing to hydrogen bonding and electron donation.[37] Additionally, the thiophene-Schiff base ligands coordinated metals with the azomethine N and thienyl S to enhance the activity.[38] The presence of a methyl group in the

Table 1 Diameter of the inhibition zones (mm) of synthesized compounds **2a–2k**, ceftriaxone (**Cef**), and amphotericin B (**Am**) against tested bacterial and fungal strains

	Gram-positive bacteria				Gram-negative bacteria		Fungi	
Compd	*S. aureus*	*B. megaterium*	*B. cereus*	*B. subtilis*	*E. coli*	*S. typhi*	*T. harzianum*	*A. niger*
2a	9.2 ± 0.3	11.2 ± 0.6	13.2 ± 0.2	13.8 ± 0.6	11.5 ± 0.4	21.2 ± 0.6	20.0 ± 0.4	15.8 ± 0.6
2b	11.5 ± 0.4	8.0 ± 0.4	—	10.0 ± 0.8	13.8 ± 0.6	7.5 ± 0.4	13.0 ± 0.8	6.5 ± 0.4
2c	12.2 ± 0.2	8.0 ± 0.4	12 ± 0.4	12.9 ± 0.3	15.3 ± 0.5	6.8 ± 0.6	11.8 ± 0.6	10.5 ± 0.4
2d	13.8 ± 0.2	14.2 ± 0.2	8.0 ± 0.4	11.1 ± 0.3	11.7 ± 0.5	14.8 ± 0.6	15.0 ± 0.4	15.7 ± 0.5
2e	7.2 ± 0.2	11.0 ± 0.8	15.0 ± 0.8	8.3 ± 0.5	11.7 ± 0.5	9.8 ± 0.6	13.5 ± 0.4	17.8 ± 0.6
2f	13.4 ± 0.4	13.9 ± 0.3	15.2 ± 0.8	17.2 ± 0.2	13.0 ± 0.8	15.2 ± 0.6	20.2 ± 0.6	32.3 ± 0.5
2g	7.5 ± 0.4	14.8 ± 0.6	11.9 ± 0.3	—	13.2 ± 0.6	14.0 ± 0.8	12.0 ± 0.4	27.7 ± 0.5
2h	17.3 ± 0.2	6.7 ± 0.5	11.0 ± 0.8	15.2 ± 0.2	8.7 ± 0.5	15.0 ± 0.8	18.7 ± 0.5	15.8 ± 0.6
2i	13.2 ± 0.2	7.7 ± 0.5	12.2 ± 0.6	11.9 ± 0.1	8.5 ± 0.4	11.8 ± 0.6	15.7 ± 0.5	12.1 ± 0.3
2j	8.3 ± 0.2	11.9 ± 0.4	13.1 ± 0.4	8.3 ± 0.5	10.3 ± 0.5	6.0 ± 0.8	11.7 ± 0.5	11.2 ± 0.6
2k	17.2 ± 0.2	9.8 ± 0.6	13.1 ± 0.3	12.9 ± 0.7	7.7 ± 0.5	14.0 ± 0.4	16.0 ± 0.8	21.8 ± 0.6
Cef	40.2 ± 0.6	50.2 ± 0.6	20.2 ± 0.6	20.0 ± 0.4	38.0 ± 0.8	44.3 ± 0.5		
Am							17.2 ± 0.6	8.0 ± 0.8
DMSO	—	—	—	—	—	—	—	—

thiophene ring might be responsible for the robust performance in this experiment. In the first series of new analogs **2a–e**, the zone of inhibition was not so pronounced against the Gram-positive bacteria, except for **2e** against *B. cereus* (15.0 ± 0.8 mm). In the case of the Gram-negative bacterial strains, compounds **2a** and **2c** displayed a maximum inhibitory growth against *S. typhi* (21.2 ± 0.6 mm) and *E. coli* (15.3 ± 0.5 mm), respectively, compared to the standard ceftriaxone (44.3 ± 0.5 and 38.0 ± 0.8 mm, respectively). On the contrary, the second series of the analogs (**2f–k**) showed some leading activities against all four Gram-positive bacterial strains, where compound **2f** exhibited maximum activity against two bacterial strains, namely *B. cereus* (15.2 ± 0.8 mm) and *B. subtilis* (17.2 ± 0.2 mm). In addition, compound **2h** showed the highest inhibitory value against *S. aureus* (17.3 ± 0.2 mm), and **2g** had the lead activity against *B. megaterium* (14.8 ± 0.6 mm). The substituted phenyl ring in compound **2f** might be responsible for its higher activity against all the bacterial strains.[36] In compounds **2g** and **2h**, the substituted methyl and methoxy groups in the phenyl ring might be accountable for their enhanced activities.[39] The nitro-substituted **2i** and **2j** showed the least activity against all the strains, while the electron-withdrawing chloro group was noticeably active, especially against *S. aureus* and the two fungal strains.

For the two fugal strains, the synthesized derivatives exhibited increased activities compared to the standard amphotericin B. Compounds **2a** (20.0 ± 0.4 mm), **2f** (20.2 ± 0.6 mm), and **2h** (18.7 ± 0.5 mm) displayed outstanding activity against the fungal strain, *T. harzianum*, compared with the standard (17.2 ± 0.6 mm). Additionally, **2d**, **2i**, and **2k** showed moderate inhibitory capability. In the case of *A. niger*, all the derivatives had a higher zone of inhibition than the standard (8.0 ± 0.8 mm), except for compound **2b**. However, the phenyl-substituted compound **2f** displayed a maximum activity of 32.3 ± 0.5 mm, four-fold higher than the standard.

3.3 Antioxidant activity

The antioxidant potency of the synthesized derivatives was determined using the DPPH free radical scavenging assay. Five different concentrations were used in this experiment, and the percentage of inhibition of the derivatives at these concentrations is represented in Fig. 2, where all the compounds revealed their maximum inhibitory value at 250 μg mL^{-1}. Among all the derivatives, **2b** and **2c** inhibited more than 80% of the DPPH free radicals at 60, 125, and 250 μg mL^{-1}. Considering the IC_{50} value of the synthesized analogs, **2c** exhibited excellent antioxidant activity with an IC_{50} value of 14.78 ± 2.73 μg mL^{-1}, having methyl and ethoxycarbonyl groups attached to the 4- and 5-position of the thiazole ring, respectively. With the presence of the thiazole-Schiff bases, the antioxidant mechanism increased along with the ability to donate hydrogen to radicals, to modulate the redox systems, and to stabilize the radical species *via* conjugation.[40] When the methyl group in the 4-position was replaced with an acetyl group in compound **2b**, it became the second most potent antioxidant agent with an IC_{50} value of 31.10 ± 3.57 μg mL^{-1} (Table 2). However, in compounds **2a**, **2d**, and **2e**, the 5-position was replaced with a hydrogen atom, and the 4-position was replaced with ethyl acetate (**2a**), pyridine (**2d**), and coumarin (**2e**), which decreased the antioxidant capability as follows: **2e** > **2a** > **2d**. In the second series of compounds (**2f–k**), the electron-withdrawing nitro group as a substituent of the phenyl ring exhibited the lowest antioxidant activity. Surprisingly, the nitro group in the para position increased the inhibitory value of compound **2j** (89.96 ± 1.52 μg mL^{-1}) compared with the *meta*-substituted nitro group in compound **2i** (152.94 ± 1.88 μg mL^{-1}). The presence of the chloro group in compound **2k** also decreased its potential as an antioxidant agent. The phenyl ring with no substituents or with methyl or methoxy groups displayed moderate activities in compounds **2f** (85.50 ± 2.19 μg mL^{-1}), **2g** (91.25 ± 2.81 μg mL^{-1}), and **2h** (90.62 ± 1.17 μg mL^{-1}) compared to the IC_{50} value of the standard ascorbic acid (49.67 ± 4.63 μg mL^{-1}).

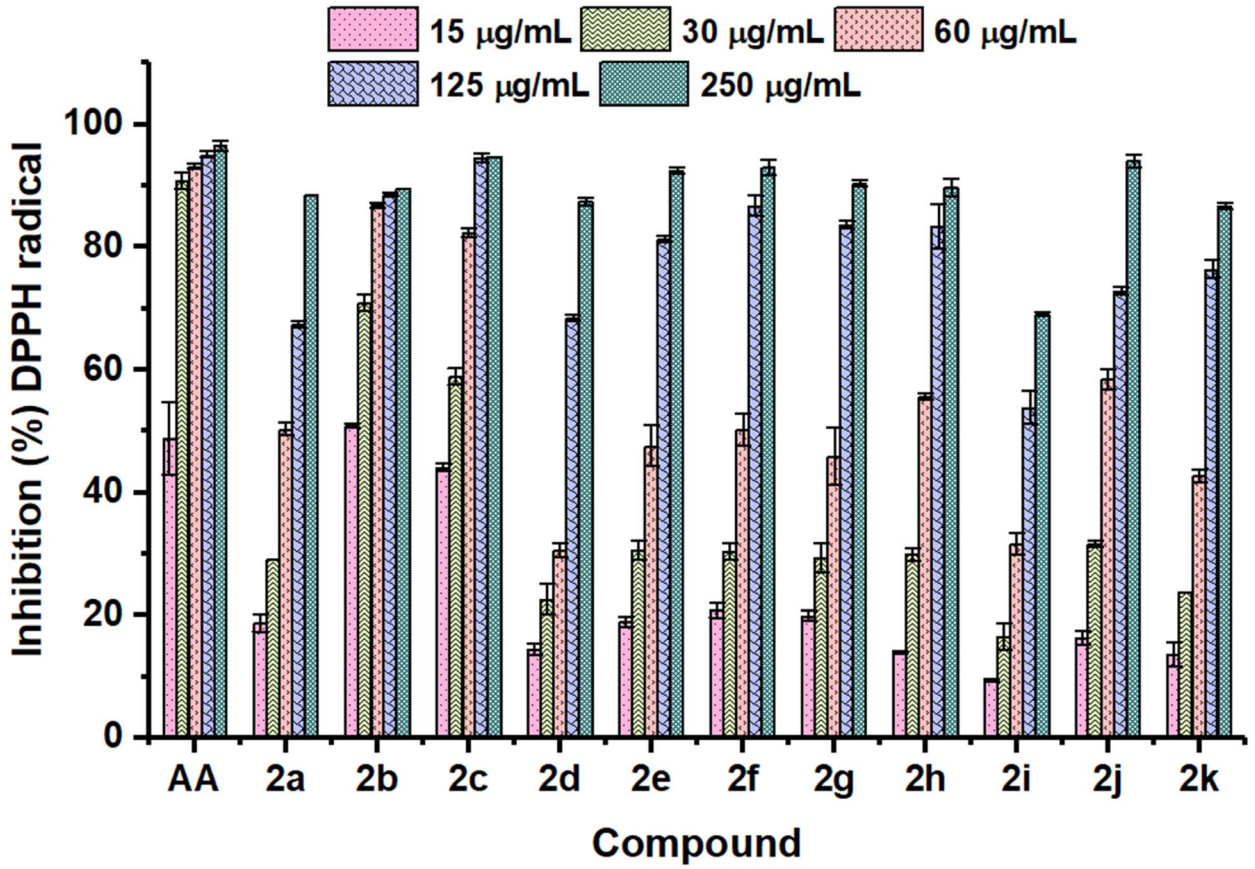

Fig. 2 Comparison of the inhibition (%) of the DPPH radicals at various concentrations of ascorbic acid (AA) and the synthesized compounds (2a–k). The data are expressed as mean ± SD of the three experiments.

Table 2 Antioxidant activities of the synthesized derivatives 2a–k and ascorbic acid. Data represent mean ± SD of three experiments

Compound	IC_{50} (μg mL^{-1})	Compound	IC_{50} (μg mL^{-1})
2a	97.75 ± 0.51	**2g**	91.25 ± 2.81
2b	31.10 ± 3.57	**2h**	90.62 ± 1.17
2c	14.78 ± 2.73	**2i**	152.94 ± 1.88
2d	114.47 ± 1.62	**2j**	89.96 ± 1.52
2e	88.89 ± 3.02	**2k**	106.37 ± 3.49
2f	85.50 ± 2.19	Ascorbic acid	49.67 ± 4.63

3.4 Computational studies

3.4.1 Molecular docking study. The interaction profile of the synthesized derivatives within a receptor is crucial for predicting their proficiency as bioactive agents. Therefore, molecular docking was performed for demonstrating their stability and binding strength with various amino acid residues. Based on the high activity of compounds **2a**, **2f**, and **2c**, respectively, as antibacterial, antifungal, and antioxidant agents, four different protein co-crystals were selected for this computational experiment. The binding interactions of the synthesized analogs with protein residues are illustrated in Fig. 3. Compound **2a** was docked against 3G1T (protein co-crystal of *S. typhi*) with a binding affinity of −7.5 kcal mol^{-1}, where the thiazole-substituted $CH_2COOCH_2CH_3$ group showed only a conventional hydrogen bond with Ser155 at 1.97 Å, along with a carbon–hydrogen bond with Gly198. Met204 and Trp164 exhibited two pi–sulfur interactions with thiazole ring at a distance of 5.47 Å and 5.71 Å. Additionally, a pi–pi T-shaped bond was formed between the thiazole ring and Tyr167. Additionally, the thiophene ring displayed two different interactions with Met204 (4.99 Å) and Ile26 (2.53 Å). The presence of a methyl group in the thiophene ring developed an alkyl interaction with the residue Ile26 at a distance of 4.04 Å. Compound **2f** was docked against two different protein co-crystals, given its high activity against *B. subtilis* (8ARE) and *A. niger* (5LWX), yielding binding affinities of −8.6 kcal mol^{-1} and −7.4 kcal mol^{-1}, respectively. In complex **2f–8ARE**, the thiophene ring revealed extended connections through four different bonds, where two interactions occurred with the ring and the double pi–alkyl interactions were involved with the methyl substituent. A pi-donor hydrogen bond and a pi–pi T-shaped bond were exhibited by the thiophene ring with Leu427 (2.97 Å) and Trp426 (5.21 Å). On the other hand, the thiophene-substituted methyl group had two pi–alkyl interactions with Try168 and Phe167. A single pi–sulfur bond was found between the thiazole ring and Arg423 at a distance of 4.19 Å. Lys27 exhibited a pi–alkyl connection with the phenyl ring at 4.99 Å. When **2f** interacted with 5LWX, an electrostatic bond was formed by the thiazole ring with

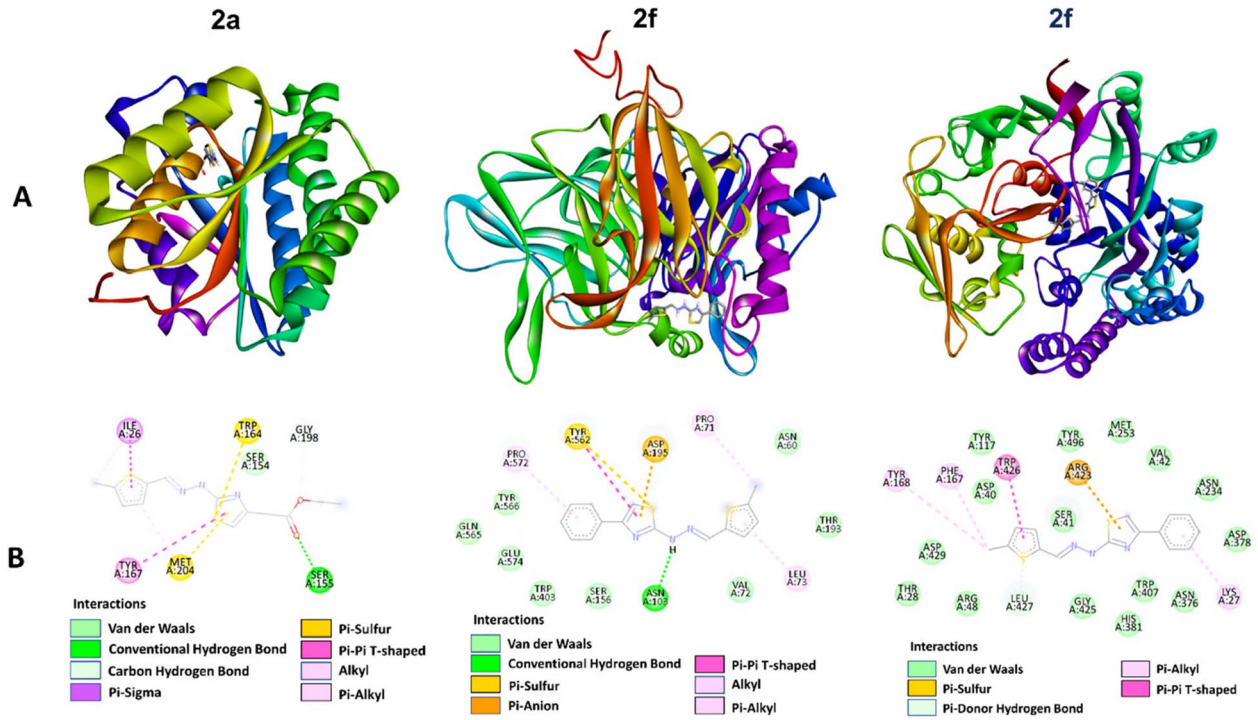

Fig. 3 Diagram of molecular docking studies of **2a** against **3G1T** and **2f** against **5LWX** and **8ARE** protein receptors. (A) 3D interaction profile and (B) 2D docking simulations.

Asn103 from 2.41 Å. Additionally, the thiazole ring was involved in two different bonds with Tyr562 at a distance of 5.42 Å (pi–sulfur) and 5.49 Å (pi–pi T-shaped). A single conventional hydrogen bond was found for the NH group of the Schiff base with Asn103 from 2.41 Å. Two pi–alkyl interactions were observed between Pro572 and the phenyl ring and between Leu73 and the thiophene ring, respectively. At a distance of 4.56, an alkyl bond was visualized between Pro71 and the thiophene-containing CH_3 group.

In the final complex **2c–2CDU**, compound **2c** demonstrated the highest antioxidant potency among all the synthesized derivatives, and was further used for the docking studies against the human antioxidant enzyme receptor 2CDU (Fig. 4). Amino acid residues exhibited plenty of interactions with

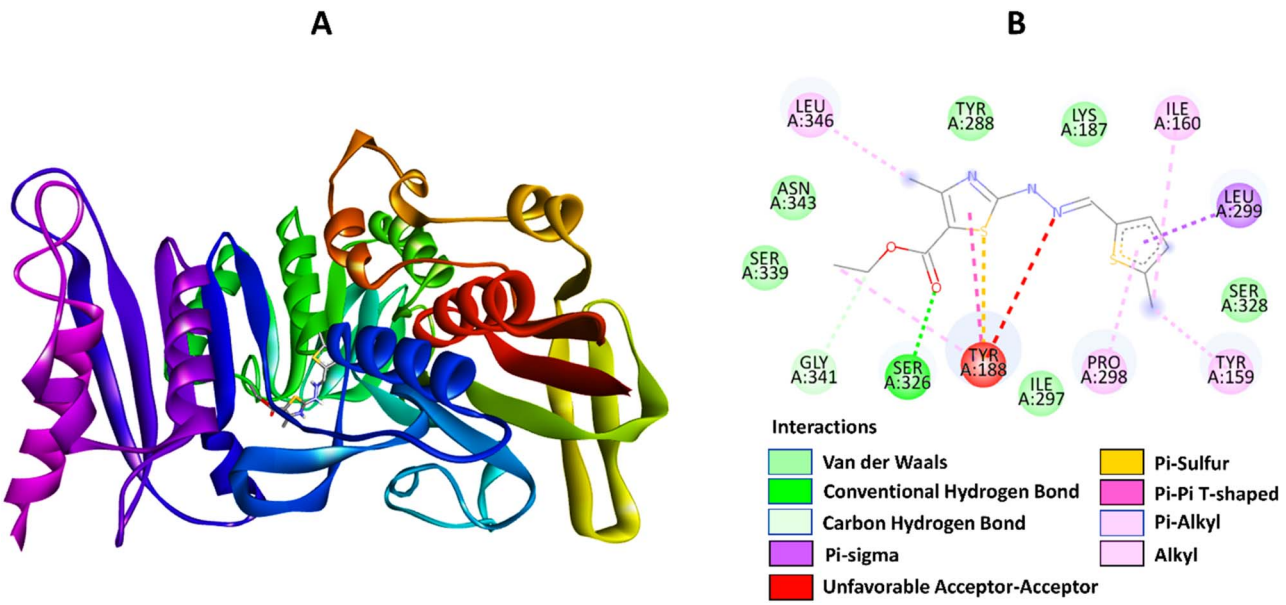

Fig. 4 Molecular docking studies of **2c** against human antioxidant enzyme receptor (PDB ID: **2CDU**). (A) 3D interaction profile and (B) 2D docking simulation.

compound **2c**, having a binding affinity of −6.6 kcal mol^{-1}. For $COOCH_2CH_3$, there was a conventional hydrogen bond between CO and Ser326, a carbon–hydrogen bond between CH_2 and Gly341, and a pi–alkyl interaction between CH_3 and Tyr188. Residue Tyr188 displayed two other interactions, as well with the thiazole ring from 4.55 Å (pi–sulfur) and 4.81 Å (pi–pi T-shaped). The thiazole ring containing the CH_3 group had an alkyl interaction at a distance of 4.08 Å with Leu346. Another Leu residue exhibited a pi–sigma bond with the thiophene ring from a distance of 5.15 Å. The thiophene ring was assumed to have a pi–alkyl interaction with Pro298 at a distance of 5.32 Å, while the methyl substituent in the ring exhibited two hydrophobic interactions with Ile160 (5.41 Å) and Typ159 (4.59 Å).

3.4.2 *In silico* ADMET properties. Absorption, distribution, metabolism, and excretion (ADME) properties were evaluated for understanding the efficacy and safety of a drug by assessing its pharmacokinetics within the body. Furthermore, the potential toxicological spectrum of the new derivatives was predicted for proving the suitability of the analogs for clinical use. Tables 3 and 4 summarize the ADME properties and toxicological parameters, respectively. Lipinski's rule of five and Veber's rule were used to evaluate the oral bioavailability of a drug, considering some key criteria, like the molecular weight, lipophilicity, hydrogen bond donors, hydrogen bond acceptors, number of rotatable bonds, and topological polar surface area. An orally active drug should not violate more than one of the mentioned criteria, and all the synthesized derivatives followed the standard criteria of Lipinski's and Veber's rules. The molecular weight of the compounds was below the range of 500 Daltons; all of them donated a single hydrogen bond and possessed 2 to 4 hydrogen bond acceptors. Compound **2a** showed a lipophilicity value of 3.03, which was the lowest among the synthesized compounds, indicating its high solubility and hydrophilic nature. The sum of the surface contribution of the polar atoms (TPSA) was excellent and suggested good oral absorption. Compounds **2f**, **2g**, and **2k** showed a TPSA value of 93.76 Å^2, indicating strong absorption and higher membrane permeability.

Table 4 *In silico* toxicity risks and drug-likeness of compounds **2a–k**, ceftriaxone (**Cef**), amphotericin B (**Am**), and ascorbic acid (**AA**). Toxicity effects are shown as M, mutagenic; T, tumorigenic; I, irritant; and R, reproductive

	Toxicity				
Compd.	M	T	I	R	Druglikeness
2a	Low	High	Low	Low	−5.11
2b	Low	High	Low	Low	4.55
2c	Low	High	Low	Low	0.96
2d	Low	High	Low	Low	5.75
2e	Low	High	Low	Medium	6.29
2f	Low	High	Low	Low	5.26
2g	Low	High	Low	Low	4.04
2h	High	High	Low	Low	5.26
2i	Low	High	Low	Low	−0.06
2j	Low	High	Low	Low	−5.1
2k	Low	High	Low	Low	5.42
Cef	Low	Low	Low	Low	16.69
Am	Low	Low	Low	Low	0.14
AA	High	High	Low	High	0.02

Human intestinal absorption (HIA) and blood–brain barrier (BBB), two crucial pharmacokinetic behaviors for drug discovery, were calculated and the results are illustrated in Fig. 5. This graph indicates the good permeation of the compounds across the membrane, which could easily reach the hepatic portal vein.[41] Except for **2a** (88%), the HIA values for all the compounds were more than 90%, even 99% for compounds **2e**, **2f**, **2h**, and **2k**. These computed values indicate their good absorption by the human intestinal cavity. All the synthesized derivatives showed positive BBB values, marking their smooth permeation through the blood–brain barrier, and the range was below 1, predicting CNS (central nervous system) inactivity.[42]

Table 3 Predicted pharmacokinetic properties of compounds **2a–k**, ceftriaxone (**Cef**), amphotericin B (**Am**), and ascorbic acid (**AA**)

		Lipinski's rule				Veber's rule			
Compd.	Lipinski's violations	MW[a] (≤500)	HBA[b] (≤10)	HBD[c] (≤5)	*c* log *P*[d] (≤5)	NROTB[e] (≤10)	TPSA[f] (140 Å^2)	Log *S*[g]	%ABS[h]
2a	0	309.41	4	1	3.08	7	120.06	−3.88	67.47
2b	0	279.38	3	1	3.11	4	110.83	−4.07	70.66
2c	0	309.41	4	1	3.49	6	120.06	−4.42	67.47
2d	0	300.40	3	1	3.37	4	106.65	−4.49	72.11
2e	0	367.44	4	1	4.25	4	123.97	−5.58	66.12
2f	0	299.41	2	1	4.11	4	93.76	−5.16	76.57
2g	0	313.44	2	1	4.45	4	93.76	−5.45	76.57
2h	0	329.44	3	1	4.10	5	102.99	−5.21	73.38
2i	0	344.41	4	1	3.35	5	139.58	−5.19	60.72
2j	0	344.41	4	1	3.36	5	139.58	−5.19	60.72
2k	0	368.30	2	1	5.17	4	93.76	−6.32	76.57
Cef	1	331	5	2	−1.53	3	72.88	−3.32	83.85
Am	1	416	3	0	4.85	6	27.05	−5.08	99.67
AA	0	176	6	4	−2.46	2	107.2	−0.35	71.91

[a] Molecular weight. [b] Number of hydrogen bond acceptors. [c] Number of hydrogen bond donors. [d] Lipophilicity. [e] Number of rotatable bonds. [f] Topological polar surface area. [g] Solubility parameter. [h] Percentage of absorption.

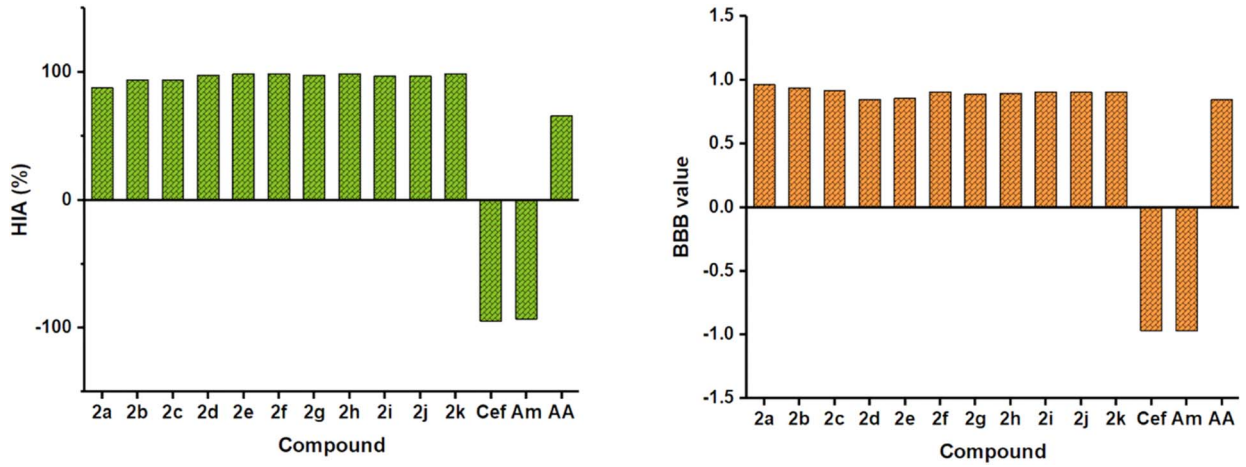

Fig. 5 Predicted HIA (%) and BBB values of synthesized derivatives **2a–k** and standard ceftriaxone (**Cef**), amphotericin B (**Am**) and ascorbic acid (**AA**).

The toxicity fillers of the synthesized derivatives are represented as M (mutagenicity), T (tumorigenicity), I (irritancy), and R (reproductive effects), which are tabulated along with the druglikeness of the synthesized derivatives in Table 4. Except for compound **2h**, all the other derivatives showed low mutagenicity. In addition, the coumarin-containing compound **2e** exhibited the highest druglikeness value of 6.29, although it had a medium reproductive effect. In the case of the drug score (Fig. 6), a maximum similarity of 0.34 and 0.33 was calculated for compounds **2b** and **2d**, respectively. The highest wet-lab active compound, **2f**, had a drugscore of 0.25, while the minimum value (0.13) belonged to compound **2j**.

3.4.3 Molecular dynamics (MD) simulation. MD simulation is a quantum leap in drug discovery for investigating the stability of ligand–protein complexes along a trajectory that accelerates the evolution of new therapeutics, increases drug efficacy, and introduces challenges like drug resistance.[43] The rigid structure of protein–ligand complexes in molecular docking requires advanced study for illustrating their dynamic behaviors and interactions at the atomic level during ligand binding within the protein active site. The MD simulation depicts various parameters, such as the RMSD (root mean square displacement), RMSF (root-mean-square fluctuation), and the radius of gyration, related to the drug-receptor interactions for a deeper understanding of the complexes. Snapshots at 5 ns intervals of the four complexes are depicted and represented in Fig. 7–10. It was observed that the ligand was strongly bound within the respective protein structures. In complex **2a–3G1T**, the ligand deviated from the active site between 15 ns and 20 ns. However, it returned to the stable position at the end of the simulation period (Fig. 7). In complexes **2f–5LWX** and **2c–2CDU**, the ligand deviated occasionally during the simulation, but was held at the active site of the receptors, while complex **2f–8ARE** displayed the most stability within the complex during the whole trajectory.

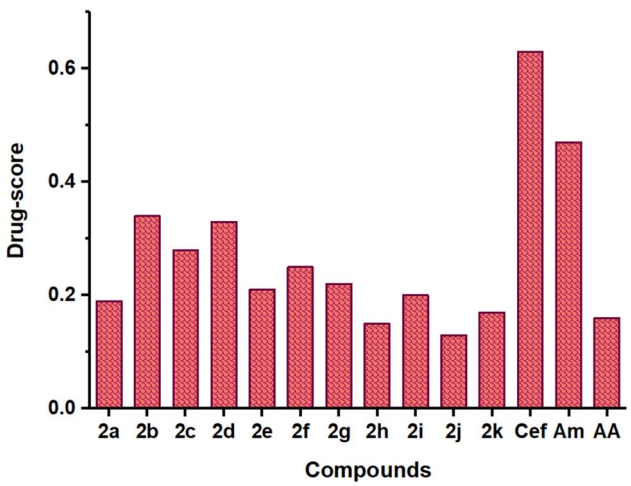

Fig. 6 Predicted drug-score of the synthesized compounds **2a–k**, ceftriaxone (**Cef**), amphotericin B (**Am**), and ascorbic acid (**AA**).

The RMSD value was used to estimate the stability of the complex, considering the deviation of the protein structure from the reference structure after ligand binding. In the **2a–3G1T** complex, the initial RMSD value was 0.36 Å, which rose to 1.14 Å at 0.8 ns, and at 2.4 ns, it again elevated to 1.17 Å, then decreased to 1.13 Å at 4.2 ns. The maximum RMSD value of 1.9 Å was observed at 5.5 ns and then dropped to 1.3 Å at 6 ns. During the trajectory, the complex maintained an average value of 1.36 Å, indicating its stability inside the receptor.[44,45] In the case of the **2f–8ARE** complex, the RMSD value was elevated from 0.36 Å to 1.00 Å at 4 ns, maintaining a mean value of 0.99 Å for the 25 ns simulation time. The maximum deviation occurred at 22 ns with an RMSD value of 1.32 Å; thus, the **2f–8ARE** complex became the most stable complex among the four complexes. On the contrary, the second complex of compound **2f** (**2f–5LWX**) showed more deviation from the reference with an average RMSD value of 1.96 Å. This complex rocketed from 0.43 to 2.01 Å at 6 ns, and at 15 ns, 20% of the RMSD values crossed 2.00 Å. However, 16–22 ns was the maximum range, and at 2.63 Å, there was the highest fluctuation. For the antioxidant-

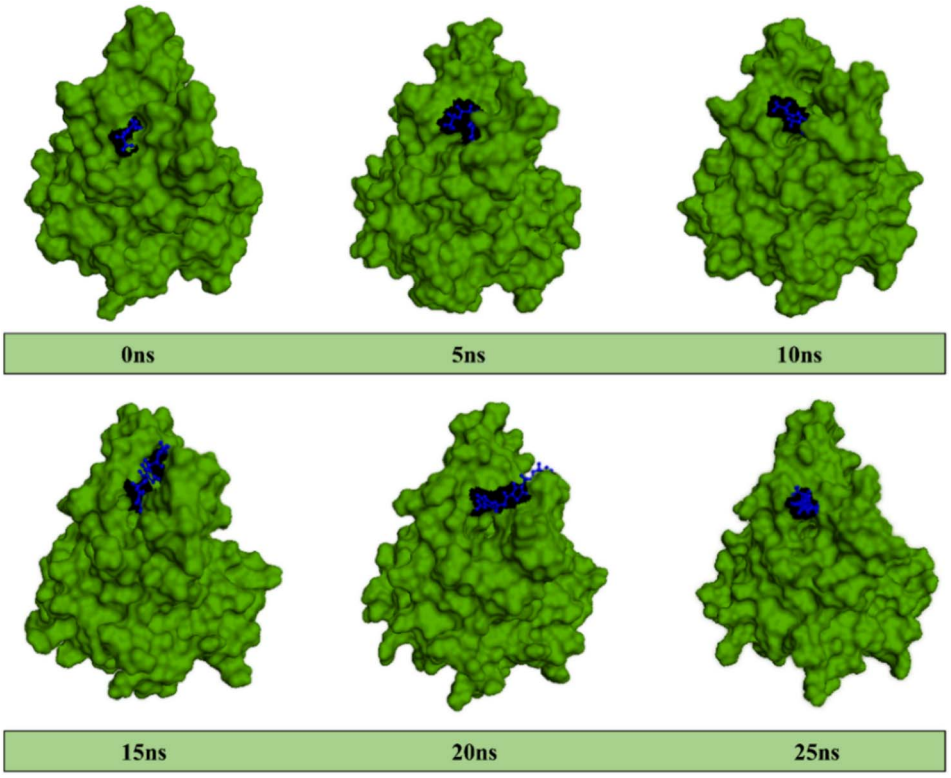

Fig. 7 MD-simulated snapshots of complex **2a–3G1T** during the 25 ns trajectory time.

active complex **2c–2CDU**, the maximum deviation was raised to 1.8 ns at 7.2 ns, making it the third-most stable complex. Initially, the RMSD value was 0.43 Å and it increased to 1.3 Å within 1 ns. After the maximum RMSD value at 7.2 ns, this complex maintained the range between 1.3–1.6 Å, with a mean value of 1.23 Å.

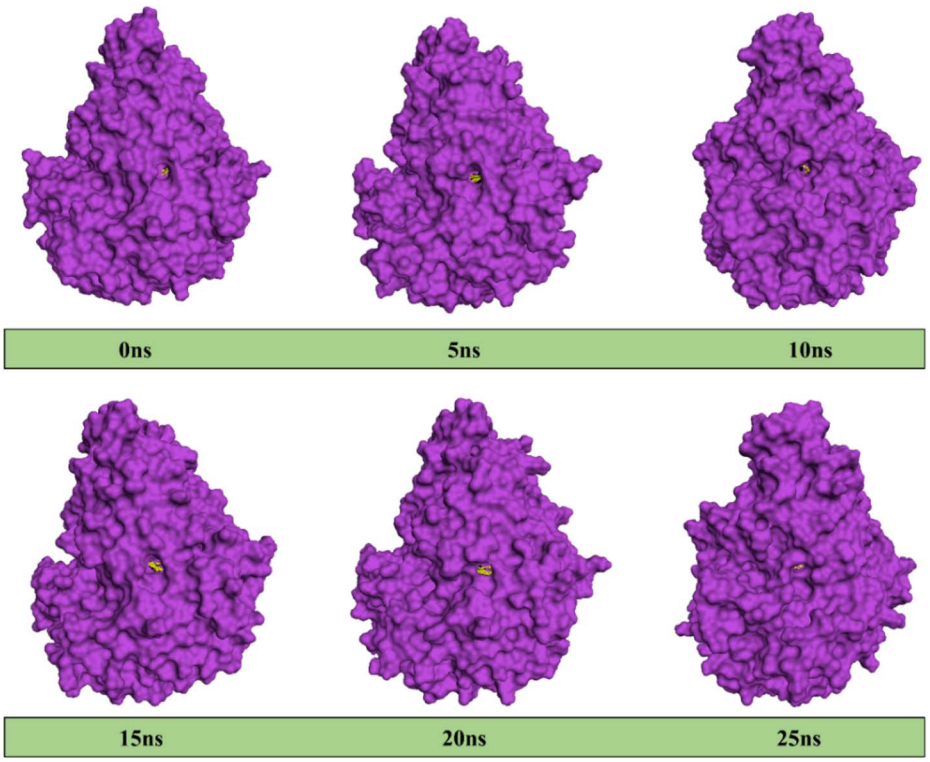

Fig. 8 MD-simulated snapshots of complex **2f–8ARE** during the 25 ns trajectory time.

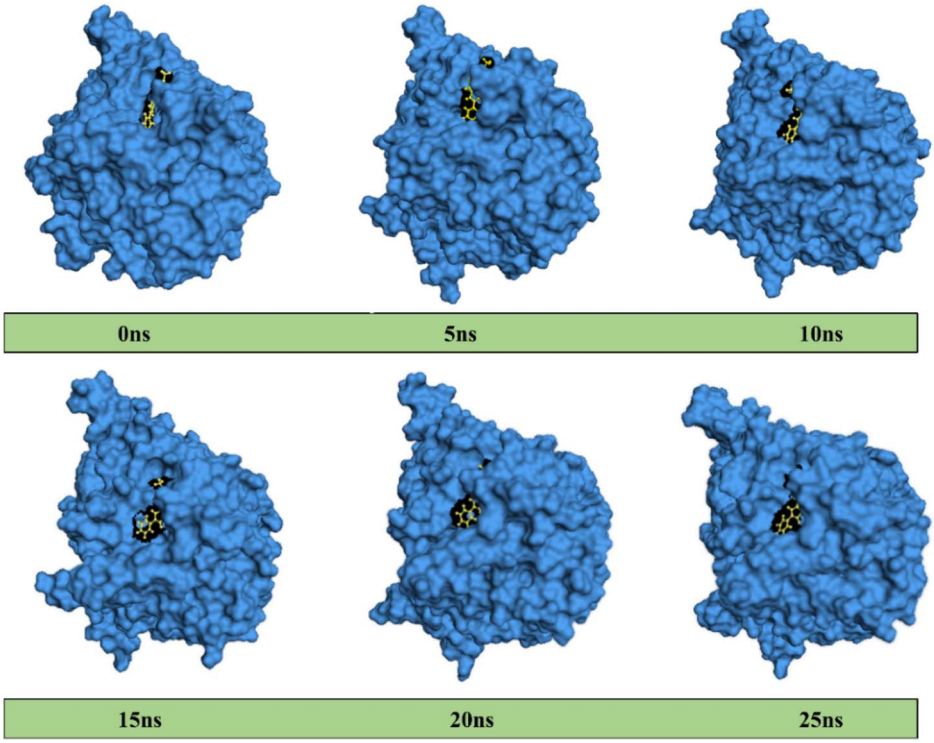

Fig. 9 MD-simulated snapshots of complex **2f–5LWX** during the 25 ns trajectory time.

RMSF measures the structural movement of amino acid from its average position after the ligand was bound inside the protein. RMSF analysis was assessed and the results are illustrated in Fig. 11 and 12 for the four complexes. The figure displays that in the **2a–3G1T** complex, Gly252 and Asn25 exhibited a minimum fluctuation of 0.423 Å, while Lys75

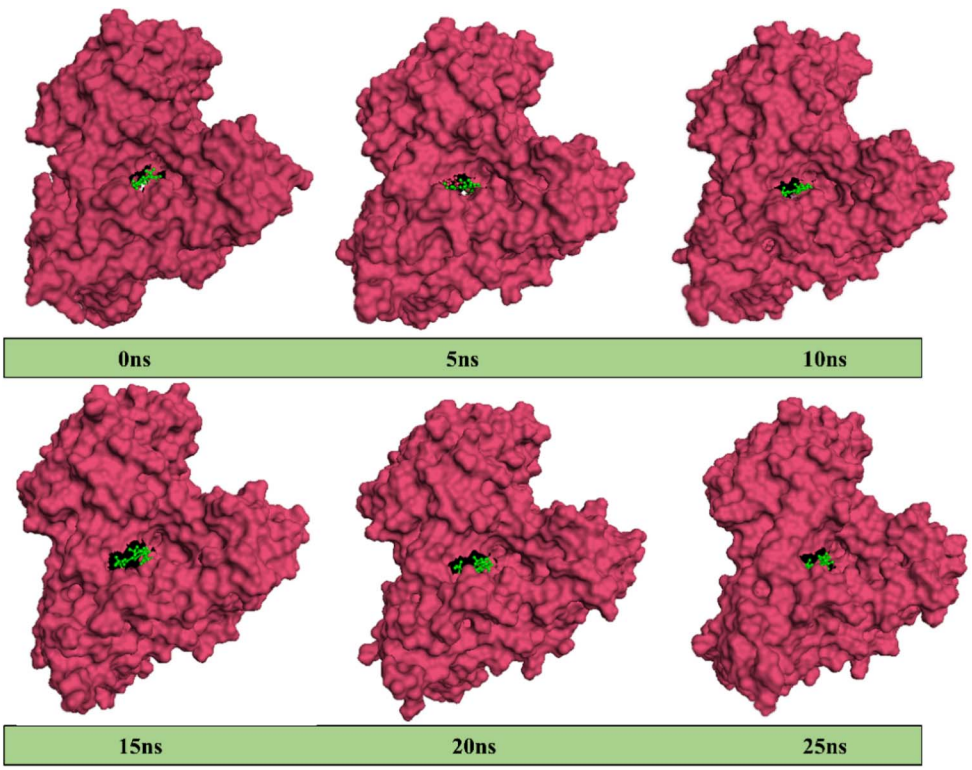

Fig. 10 MD-simulated snapshots of complex **2c–2CDU** during the 25 ns trajectory time.

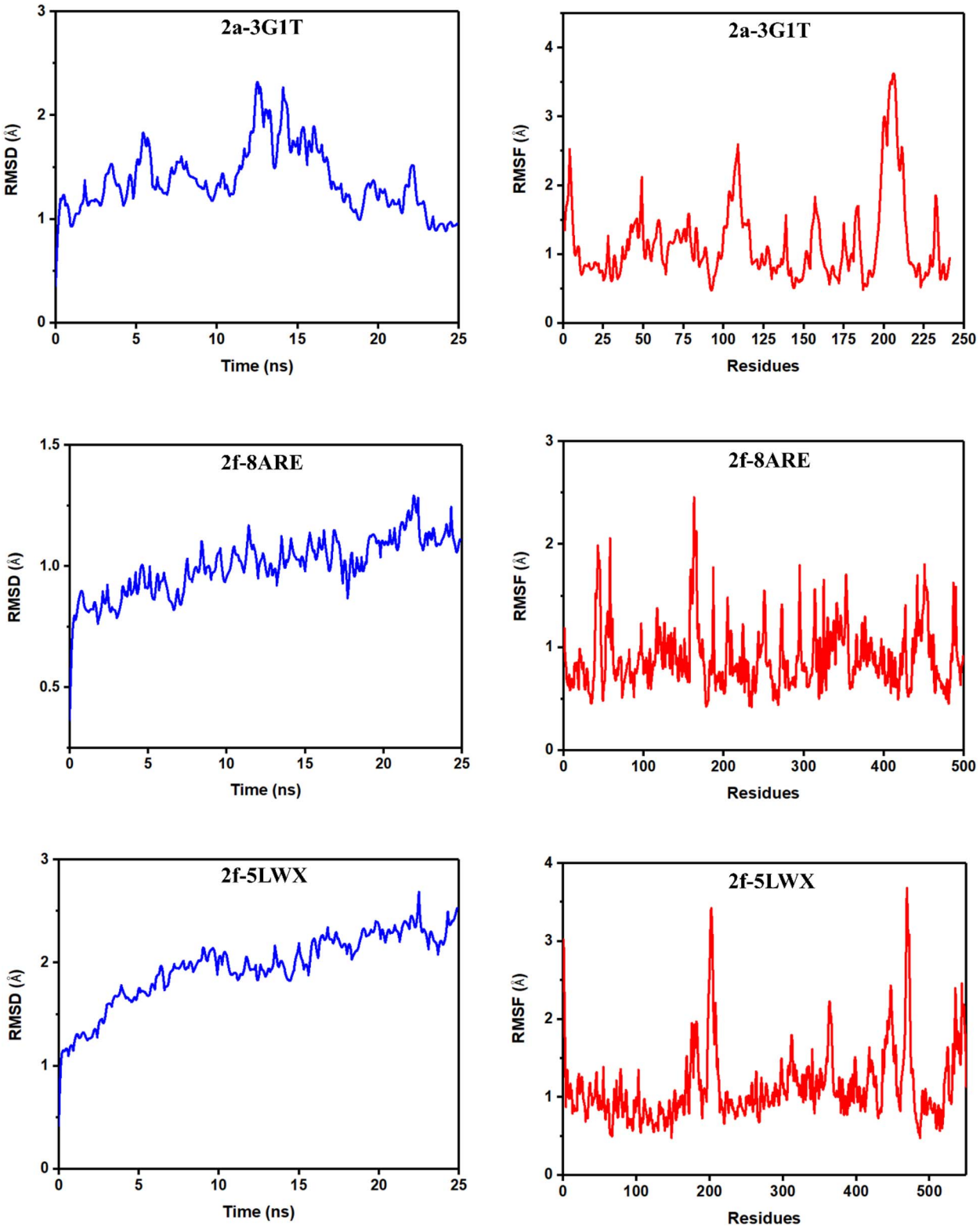

Fig. 11 RMSD and RMSF plots for the three protein–ligand systems **2a–3G1T**, **2f–8ARE**, and **2f–5LWX** with respect to equilibrated initial structure.

displayed a maximum RMSF value of 2.058 Å. The lysine residues exhibited fluctuations in the range of (1–1.8) Å, which implies that the lysine residues were less flexible. However, most of the amino acid residues were stable and fluctuated within the 0.4–0.8 Å range. In the **2f–8ARE** complex, Lys280 revealed a maximum fluctuation of 2.457 Å and Asn25 showed

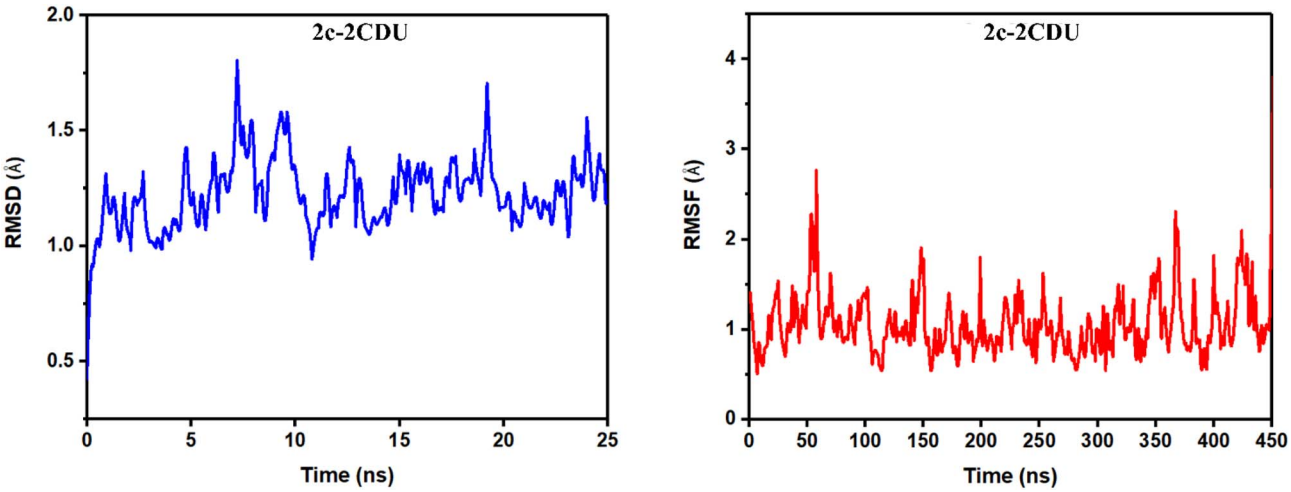

Fig. 12 RMSD and RMSF plots for **2c–2CDU** complex with respect to the equilibrated initial structure.

a minimum fluctuation of 0.423 Å. Lys102, Lys103, Glu62, and Lys226 showed fluctuations above 1.4 Å, and threonine exhibited minimal fluctuations above 1.1–1.3 Å. When the **2f** compound was bound with the **5LWX** protein, it exhibited maximum fluctuations of 3.367 Å and 3.422 Å due to Asp225 and the root mean square of the structure. The Trp88 residue revealed a minimum fluctuation of 0.511 Å. Most of the residues exhibited fluctuations in the range of 0.5–0.8 Å, indicating their relative stability. In the case of the **2c–2CDU** complex, Lys150 and Arg58 showed maximum fluctuations of 2.67 Å and 2.77 Å, respectively, indicating less flexibility. Ty201, Gly180, Asp179, and Gly156 showed fluctuations of about 0.5 Å. Gly7 exhibited a minimum fluctuation value of 0.508 Å.

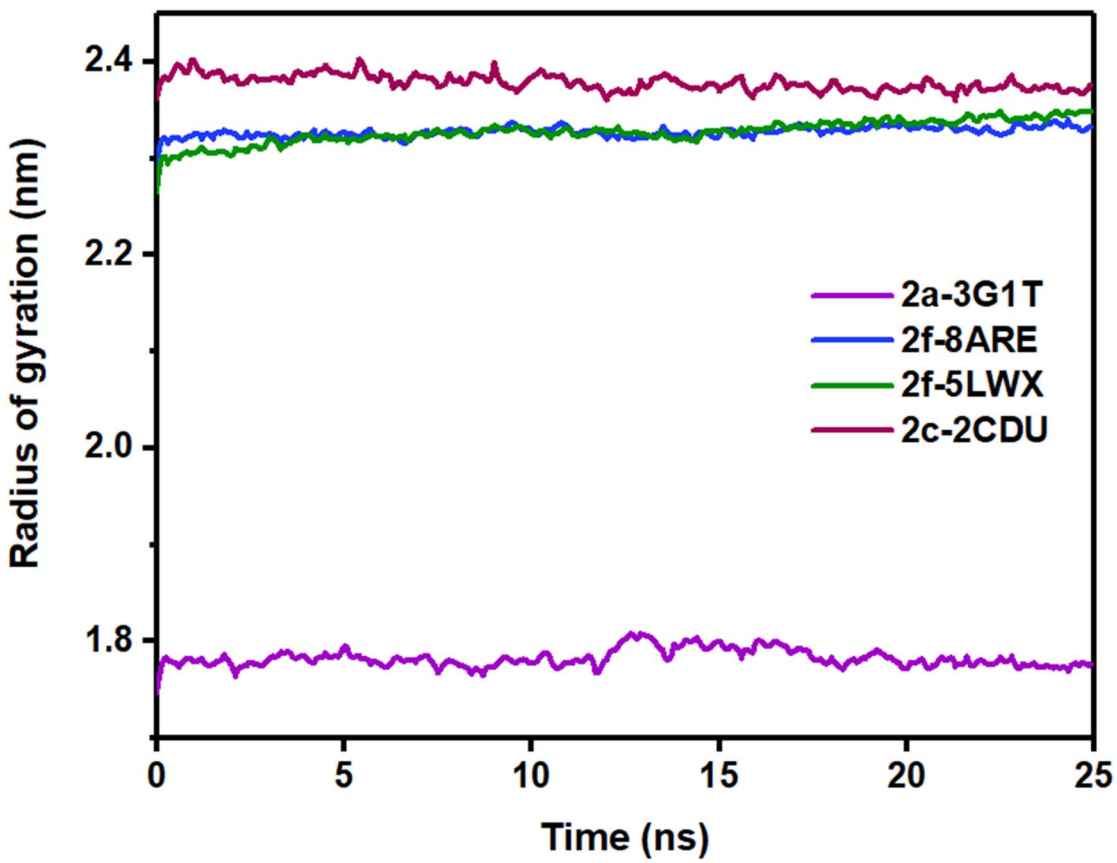

Fig. 13 Radius of gyration (R_g) plot against the simulation time of 25 ns for **2g** + **8DAI**, **2g** + **2YOK**, and **2d** + **2CDU**.

A radius of gyration (R_g) analysis was employed to understand the compactness and extension of the ligand–protein complex during the simulation. The R_g (nm) *vs.* time (ns) plot is presented in Fig. 13. The figure demonstrates that the R_g value of the **2f** + **8ARE** complex ranged from 22.96 Å to 23.408 Å. In the **2a** + **3G1T** complex, the R_g value remained in the range of 17.46 to 17.99 Å, and that of the **2f** + **5LWX** complex ranged from 22.66 Å to 23.49 Å. In the **2c** + **2CDU** complex, the R_g value was 23.625 to 24 Å. These results are consistent with those executed with the MD simulations, certifying the stability of the interaction between the detected compounds and the protein receptors.[46,47]

4. Conclusions

The synthesis of eleven thiazole-Schiff base derivatives was achieved by a two-step reaction. The chemical structures were confirmed by spectral analysis (IR, ^{1}H NMR, and HRMS). The biological studies showed that the novel **2f** derivative had an outstanding antimicrobial activity. In terms of antioxidant activity, compound **2c** revealed a relatively higher capability as an antioxidant agent. Based on the initial microbiological screening outcomes, molecular docking was performed to evaluate the interaction between the promising novel derivatives and the target proteins. The results indicated that compounds **2a**, **2f**, and **2c** showed stable binding interactions with the receptor proteins. Further, the MD simulation results fortified the stability of the ligand during the simulation. The experimental *in vitro* results agreed well with the theoretical outcomes of the *in silico* studies. Overall, from this study, novel thiazole-Schiff base derivatives can be utilized as antibiotic candidates in the future.

Author contributions

Samira Jarin Khan: data curation, formal analysis, investigation. Sumita Saznin Marufa: visualization, software, writing – original draft, writing – review & editing. Md. Imtiaz Sultan: software, writing – original draft. Alin Tasnim Aurora: formal analysis, visualization. Joya Rani Debnath: writing – review & editing. Shanta Easmin: formal analysis. Hiroshi Nishino: formal analysis. Md. Aminul Haque: conceptualization, methodology, supervision, writing – review & editing. Mohammad Mostafizur Rahman: conceptualization, methodology, fund acquisition, project administration, supervision, writing – review & editing.

Conflicts of interest

The authors declare that there is no competing interests.

Data availability

The research data associated with this article are included within the article and its supplementary information (SI). Supplementary information (SI) is available. See DOI: **https://doi.org/10.1039/d5ra07357j**.

Acknowledgements

Authors are grateful to the Ministry of Science and Technology (MOST) (Project ID: 584 Phy's, 2021-2022), Bangladesh, and Jagannath University (Project 2021-2022), Dhaka, Bangladesh, for funding this project. Authors are also indebted to the Instrumental Analysis Center, Kumamoto University, Kumamoto, Japan, for the HRMS analyses. Authors are grateful to Professor Dr Nafees Ahmed, Department of Chemistry, Jagannath University, Dhaka, Bangladesh, for his support.

References

1 D. Drozdowska, D. Maliszewski, A. Wróbel, A. Ratkiewicz and M. Sienkiewicz, New Benzamides as Multi-Targeted Compounds: A Study on Synthesis, AChE and BACE1 Inhibitory Activity and Molecular Docking, *Int. J. Mol. Sci.*, 2023, **24**(19), 14901, DOI: **10.3390/ijms241914901**.

2 Q. An, L. Huang, C. Wang, D. Wan and Y. Tu, New strategies to enhance the efficiency and precision of drug discovery, *Front. Pharmacol*, 2025, **16**, 1550158, DOI: **10.3389/fphar.2025.1550158**.

3 I. Pibiri, Recent Advances: Heterocycles in Drugs and Drug Discovery, *Int. J. Mol. Sci.*, 2024, **25**(17), 9503, DOI: **10.3390/ijms25179503**.

4 D. K. Slman, H. A. Satar, Z. A. Ketan and A. A. Jawad, Heterocyclic Compounds: A Study of its Biological Activity, *Al-Nahrain J. Sci.*, 2024, **27**(5), 19–24, DOI: **10.22401/ANJS.27.5.03**.

5 A. Petrou, M. Fesatidou and A. Geronikaki, Thiazole Ring—A Biologically Active Scaffold, *Molecules*, 2021, **26**(11), 3166, DOI: **10.3390/molecules26113166**.

6 F. Meng, Z. Yan, Y. Lu and X. Wang, Design, synthesis, and antifungal activity of flavonoid derivatives containing thiazole moiety, *Chem. Pap.*, 2023, **77**, 877–885, DOI: **10.1007/s11696-022-02522-4**.

7 A. V. Kurkin, F. Curreli, I. R. Iusupov, E. A. Spiridonov, S. Ahmed, P. O. Markov, E. V. Manasova, A. Altieri and A. K. Debnath, Design, Synthesis, and Antiviral Activity of the Thiazole Positional Isomers of a Potent HIV-1 Entry Inhibitor NBD-14270, *ChemMedChem*, 2022, **17**(22), e202200344, DOI: **10.1002/cmdc.202200344**.

8 G. Kumaraswamy, M. Ravichandar and M. Ramchander, Synthesis, In-vitro and In-silico Anti-inflammatory activity of new Thiazole derivatives, *Res. J. Pharm. Technol.*, 2021, **14**(8), 4253–4260, DOI: **10.52711/0974-360X.2021.00738**.

9 K. Narendar, B. S. Rao, S. Tirunavalli, S. S. Jadav, S. B. Andugulapati, V. Ramalingam and K. S. Babu, Synthesis of novel thiazoles bearing lupeol derivatives as potent anticancer and anti-inflammatory agents, *Nat. Prod. Res.*, 2024, **38**(13), 2207–2214, DOI: **10.1080/14786419.2023.2166042**.

10 A. Petrou, M. Fesatidou and A. Geronikaki, Thiazole Ring—A Biologically Active Scaffold, *Molecules*, 2021, **26**(11), 3166, DOI: **10.3390/molecules26113166**.

11 M. Djukic, M. Fesatidou, I. Xenikakis, A. Geronikaki, V. T. Angelova, V. Savic, M. Pasic, B. Krilovic, D. Djukic,

B. Gobeljic, M. Pavlica, A. Djuric, I. Stanojevic, D. Vojvodic and L. Saso, *In vitro* antioxidant activity of thiazolidinone derivatives of 1,3-thiazole and 1,3,4-thiadiazole, *Chem.-Biol. Interact.*, 2018, **286**, 119–131, DOI: **10.1016/j.cbi.2018.03.013**.

12 M. S. Shah, M. M. Rahman, M. D. Islam, A. A. Macktuf, J. U. Ahmed, H. Nishino and M. A. Haque, Synthesis, antimicrobial and antioxidant evaluation with in silico studies of new thiazole Schiff base derivatives, *J. Mol. Struct.*, 2022, **1248**, 131465, DOI: **10.1016/j.molstruc.2021.131465**.

13 S. Gomha, K. Khalil, H. A. Aziz and M. Abdalla, Synthesis and Antihypertensive α-Blocking Activity Evaluation of Thiazole Derivatives Bearing Pyrazole Moiety, *Heterocycles*, 2015, **91**(9), 1763–1773, DOI: **10.3987/COM-15-13290**.

14 R. M. D. da Cruz, F. J. B. Mendonça Junior, N. B. de Mélo, L. Scotti, R. S. A. de Araújo, R. N. de Almeida and R. O. de Moura, Thiophene-Based Compounds with Potential Anti-Inflammatory Activity, *Pharmaceuticals*, 2021, **14**(7), 692, DOI: **10.3390/ph14070692**.

15 G. Roman, Thiophene-containing compounds with antimicrobial activity, *Arch. Pharm.*, 2022, **355**(6), DOI: **10.1002/ardp.202100462**.

16 E. A. E. El-Helw, A. Y. A. Alzahrani and S. K. Ramadan, Synthesis and Antimicrobial Activity of Thiophene-Based Heterocycles Derived from Thiophene-2-Carbohydrazide, *Future Med. Chem.*, 2024, **16**(5), 439–451, DOI: **10.4155/fmc-2023-0304**.

17 H. Şenol and F. Çakır, 3-Amino-thiophene-2-carbohydrazide Derivatives as Anti Colon Cancer Agents: Synthesis, Characterization, In-Silico and In-Vitro Biological Activity Studies, *ChemistrySelect*, 2023, **8**(39), 1–18, DOI: **10.1002/slct.202302448**.

18 Y. A. Al-Soud, Synthesis and anti-HIV activity of substituted 1,2,4-triazolo-thiophene derivatives, *Heteroat. Chem.*, 2007, **18**(4), 443–448, DOI: **10.1002/hc.20319**.

19 B. Mathew, J. Suresh and S. Anbazhagan, Synthesis, in silico preclinical evaluation, antidepressant potential of 5-substituted phenyl-3-(thiophen-2-yl)-4,5-dihydro-1h-pyrazole-1-carboxamides, *Biomed. Aging Pathol.*, 2014, **4**(4), 327–333, DOI: **10.1016/j.biomag.2014.08.002**.

20 P. S. Mahajan, M. D. Nikam, L. U. Nawale, V. M. Khedkar, D. Sarkar and C. H. Gill, Synthesis and Antitubercular Activity of New Benzo[b]thiophenes, *ACS Med. Chem. Lett.*, 2016, **7**(8), 751–756, DOI: **10.1021/acsmedchemlett.6b00077**.

21 R. Nair, A. Shah, S. Baluja and S. Chanda, Synthesis and antibacterial activity of some Schiff base complexes, *J. Serb. Chem. Soc.*, 2006, **71**(7), 733–744, DOI: **10.2298/JSC0607733N**.

22 T. F. F. Magalhães, C. M. da Silva, L. B. F. dos Santos, D. A. Santos, L. M. Silva, B. B. Fuchs, E. Mylonakis, C. V. B. Martins, M. A. d. R. Stoianoff and Â. de Fátima, Cinnamyl Schiff bases: synthesis, cytotoxic effects and antifungal activity of clinical interest, *Lett. Appl. Microbiol.*, 2020, **71**(5), 490–497, DOI: **10.1016/j.jare.2018.06.004**.

23 S. M. Bufarwa, M. Belaidi, L. M. Abbass and D. K. Thbayh, Anticancer Activity, DFT, Molecular Docking, ADMET, and Molecular Dynamics Simulations Investigations of Schiff Base Derived From 2,3-Diaminophenazine and Its Metal Complexes, *Appl. Organomet. Chem.*, 2024, **39**(1), 7953, DOI: **10.1002/aoc.7953**.

24 S. Kaushik, S. K. Paliwal, M. R. Iyer and V. M. Patil, Promising Schiff bases in antiviral drug design and discovery, *Med. Chem. Res.*, 2023, **32**, 1063–1076, DOI: **10.1007/s00044-023-03068-0**.

25 H. Dong, J. Liu, X. Liu, Y. Yu and S. Cao, Combining molecular docking and QSAR studies for modeling the anti-tyrosinase activity of aromatic heterocycle thiosemicarbazone analogues, *J. Mol. Struct.*, 2018, **1151**, 353–365, DOI: **10.1016/j.molstruc.2017.08.034**.

26 M. Balouiri, M. Sadiki and S. K. Ibnsouda, Methods for in vitro evaluating antimicrobial activity: A review, *J. Pharm. Anal.*, 2016, **6**, 71–79, DOI: **10.1016/j.jpha.2015.11.005**.

27 S. S. Marufa, M. M. Rahman, M. M. Rahman, R. Jahan, G. Ara, H. Nishino, M. S. Alam and M. A. Haque, Synthesis, Antimicrobial and Antioxidant Activity with *in silico* ADMET Prediction, Molecular Docking and Dynamics Studies of Carbazole Ring Containing Thiazole Schiff Bases, *Asian J. Org. Chem.*, 2024, **13**(12), e202400363, DOI: **10.1002/ajoc.202400363**.

28 A. M. Hughes, J. F. Darby, E. J. Dodson, S. J. Wilson, J. P. Turkenburg, G. H. Thomas and A. J. Wilkinson, Peptide transport in Bacillus subtilis - structure and specificity in the extracellular solute binding proteins OppA and DppE, *Microbiology*, 2022, **168**, DOI: **10.1099/mic.0.001274**.

29 V. N. Malashkevich, R. Toro, J. M. Sauder, S. K. Burley, S. C. Almo, CRYSTAL STRUCTURE OF short chain dehydrogenase from Salmonella enterica subsp. enterica serovar Typhi str. CT18, New York SGX Research Center for Structural Genomics (NYSGXRC), 2009, DOI: **10.2210/pdb3G1T/pdb**.

30 M. Ferraroni, A. H. Westphal, M. Borsari, J. A. Tamayo-Ramos, F. Briganti, L. H. de Graaff and J. H. Willem van Berkel, Structure and function of Aspergillus niger laccase McoG, *Biocatalysis*, 2017, **3**(1), 1–21, DOI: **10.1515/boca-2017-0001**.

31 G. T. Lountos, R. Jiang, W. B. Wellborn, T. L. Thaler, A. S. Bommarius and A. M. Orville, The Crystal Structure of Nad(P)H Oxidase from Lactobacillus Sanfranciscensis: Insights Into the Conversion of O(2) Into Two Water Molecules by the Flavoenzyme, *Biochemistry*, 2006, **45**(32), 9648–9659, DOI: **10.1021/bi060692p**.

32 M. Fekadu, D. Zeleke, B. Abdi, A. Guttula, R. Eswaramoorthy and Y. Melaku, Synthesis, in silico molecular docking analysis, pharmacokinetic properties and evaluation of antibacterial and antioxidant activities of fluoroquinolines, *BMC Chem.*, 2022, **16**(1), 1, DOI: **10.1186/s13065-022-00795-0**.

33 A. Haikal and A. R. Ali, Chemical composition and toxicity studies on *Lantana camara* L. flower essential oil and its *in silico* binding and pharmacokinetics to superoxide dismutase 1 for amyotrophic lateral sclerosis (ALS) therapy, *RSC Adv.*, 2024, **14**(33), 24250–24264, DOI: **10.1039/D4RA04281F**.

34 L. C. Xue, J. P. Rodrigues, P. L. Kastritis, A. M. Bonvin and A. Vangone, PRODIGY: A Web Server for Predicting the Binding Affinity of Protein–Protein Complexes, *Bioinformatics*, 2016, **32**, 3676–3678, DOI: **10.1093/bioinformatics/btw514**.

35 A. S. Salman, N. A. Mahmoud, A. Abdel-Aziem, M. A. Mohamed and D. M. Elsisi, Synthesis, Reactions and Antimicrobial Activity of Some New 3-Substituted Indole Derivatives, *Int. J. Org. Chem.*, 2015, **5**, 81–99, DOI: **10.4236/ijoc.2015.52010**.

36 M. S. Alam, J. U. Ahmed and L. Dong-Ung, Synthesis, Antibacterial, Antioxidant Activity and QSAR Studies of Novel 2-Arylidenehydrazinyl-4-arylthiazole Analogues, *Chem. Pharm. Bull.*, 2014, **62**(12), 1259–1268, DOI: **10.1248/cpb.c14-00616**.

37 F. Lemilemu, M. Bitew, T. B. Demissie, R. Eawaramoorthy and M. Endle, Synthesis, antibacterial and antioxidant activities of Thiazole-based Schiff base derivatives: a combined experimental and computational study, *BMC Chem.*, 2024, **15**, 67, DOI: **10.1186/s13065-021-00791-w**.

38 S. Yasmeen, S. H. Sumrra, M. S. Akram and Z. H. Chohan, Antimicrobial metal-based thiophene derived compounds, *J. Enzyme Inhib. Med. Chem.*, 2017, **32**(1), 106–112, DOI: **10.1080/14756366.2016.1238363**.

39 D. Ungureanu, B. Tiperciuc, C. Nastasă, I. Ionut, G. Marc, I. Oniga and O. Oniga, An Overview of the Structure–Activity Relationship in Novel Antimicrobial Thiazoles Clubbed with Various Heterocycles (2017–2023), *Pharmaceutics*, 2024, **16**, 89, DOI: **10.3390/pharmaceutics16010089**.

40 F. Lemilemu, M. Bitew, T. B. Demissie, R. Eawaramoorthy and M. Endle, Synthesis, antibacterial and antioxidant activities of Thiazole-based Schiff base derivatives: a combined experimental and computational study, *BMC Chem.*, 2021, **15**, 67, DOI: **10.1186/s13065-021-00791-w**.

41 M. D. Islam, J. K. Saha, S. S. Marufa, T. K. Kundu, I. Hossain, H. Nishino, M. S. Alam, M. A. Haque and M. M. Rahman, Synthesis, antibacterial activity, *in silico* ADMET prediction, docking, and molecular dynamics studies of substituted phenyl and furan ring containing thiazole Schiff base derivatives, *PLoS One*, 2025, **20**(3), 0318999, DOI: **10.1371/journal.pone.031899**.

42 Y. B. Laskar, P. B. Mazumder and A. D. Talukdar, *Hibiscus sabdariffa* anthocyanins are potential modulators of estrogen receptor alpha activity with favourable toxicology: a computational analysis using molecular docking, ADME/Tox prediction, 2D/3D QSAR and molecular dynamics simulation, *J. Biomol. Struct. Dyn.*, 2023, **41**(2), 611–633, DOI: **10.1080/07391102.2021.2009914**.

43 O. M. H. Salo-Ahen, I. Alanko, R. Bhadane, A. M. J. J. Bonvin, R. V. Honorato, S. Hossain, A. H. Juffer, A. Kabedev, M. L. Kakkonen, A. S. Larsen, E. Lescrinier, P. Marimuthu, M. U. Mirza, G. Mustafa, A. N. Alves, T. Pantsar, A. Saadabadi, K. Singaravelu and M. Vanmeert, Molecular Dynamics Simulations in Drug Discovery and Pharmaceutical Development, *Processes*, 2021, **9**(1), 71, DOI: **10.3390/pr9010071**.

44 S. S. Marufa, M. M. Rahman, M. M. Rahman, J. R. Devnath, M. A. Mim, R. Jahan, H. Nishino, M. S. Alam and M. A. Haque, Conventional and microwave-assisted synthesis, antimicrobial and antioxidant activity evaluation with in silico studies of carbazole-thiazole-Schiff base hybrids, *J. Mol. Struct.*, 2025, **1321**, 139861, DOI: **10.1016/j.molstruc.2024.139861**.

45 F. Akhter, S. S. Marufa, S. M. A. U. Shohag, H. Nishino, M. S. Alam, M. A. Haque and M. M. Rahman, Synthesis, antimicrobial evaluation, ADMET prediction, molecular docking and dynamics studies of pyridine and thiophene moiety-containing chalcones, *R. Soc. Open Sci.*, 2025, **12**, 241411, DOI: **10.1098/rsos.241411**.

46 M. M. Melk and A. F. El-Sayed, Phytochemical profiling, antiviral activities, molecular docking, and dynamic simulations of selected *Ruellia* species extracts, *Sci. Rep.*, 2024, **14**(1), DOI: **10.1038/s41598-024-65387-5**.

47 S. S. Marufa, T. Rahman, M. M. Rahman, M. M. Rahman, S. J. Khan, R. Jahan, H. Nishino, M. S. Alam and M. A. Haque, Design, synthesis, molecular docking, and dynamics studies of novel thiazole-Schiff base derivatives containing a fluorene moiety and the assessment of their antimicrobial and antioxidant activity, *RSC Adv.*, 2024, **14**(47), 35198–35214, DOI: **10.1039/D4RA04197F**.